Eur. Phys. J. Appl. Phys. (2013) 63: 30501
DOI: 10.1051/epjap/2013130114

THE EUROPEAN PHYSICAL JOURNAL APPLIED PHYSICS

Regular Article

Analysis on propagation properties of the eigenmodes in nonplanar ring resonators

Dong Li, Jianlin Zhao[a], Dandan Wen, and Yajun Jiang

Key Laboratory of Space Applied Physics and Chemistry, Ministry of Education, and Shaanxi Key Laboratory of Optical Information Technology, School of Science, Northwestern Polytechnical University, Xi'an 710072, P.R. China

Received: 5 March 2013 / Received in final form: 2 May 2013 / Accepted: 31 July 2013
Published online: 3 September 2013 –

Abstract. Combining with the self-consistent condition and extended 5×5 matrix, we theoretically analyzed the polarization properties of the eigenmodes throughout the nonplanar ring resonators with different structures. According to the satisfactory cross section size of the eigenmodes, a comparative study of the stability properties of these nonplanar ring resonators is also provided, and the three dimensions stability space of these resonators are presented for the first time as far as our knowledge goes. The results show that the major and minor axes of the cross section change with the propagation distance and have a symmetrical point for resonators with two different structures, and the area of the stable region for these resonators can be extended by changing the incident angles of the laser beam or the radii of mirror surfaces in the resonator. These interesting results are important for designing and arranging the diaphragm in ring resonators with a nonplanar structure, as well as optimizing the structure of the resonators themselves.

1 Introduction

Being fully autonomous, highly accurate and uninfluenced by weather conditions and backscattering originated from optically active crystal, the ring laser gyroscope (RLG) with nonplanar structure are almost ideal navigation devices which are motivating ongoing interest in inertial navigation systems (INS) community [1–3]. A nonplanar ring resonator is a closed polygonal ring, in which all the segments do not lie in a single plane [4,5]. The measurement precision of a ring laser gyroscope with nonplanar structure can be improved because of eliminating the lock-in effect without using quartz crystal, which can induce the effective bias of a gyroscope but also induce additional errors (such as loss, scattering, etc.). Some previous works focused on the polarization rotation properties of laser beam in the nonplanar ring to create more complex types of ring laser gyroscopes [6,7]. The misalignment or axis perturbation of the nonplanar ring resonators have also been analyzed [8–11]. It is well known that the resonator is the core component of a gyroscope and its parameters can affect the precision of the gyroscope evidently [12–15]. Figure 1 presents the geometrical construction of a typical nonplanar ring resonator with a total length L. Where, σ is defined as the folding angle and μ is the incident angle of the laser beam on mirror A. In this paper, we analyze the propagation properties of the eigenmodes in a general skew rhombus nonplanar ring resonators (that means the incident angles on mirrors A and C are μ_{12}, while the incident angles on mirrors B and D are μ_{23}), such as the beam size on the elliptical cross section of the eigenmodes, the wave-front (i.e., the track of the points with the same phase) radius of curvature, as well as azimuths of the beam cross section and the contour of equal phase, and discuss the stability in three dimensions of these two different nonplanar ring resonators as a function of the ratio L/r, incident angle μ and folding angle σ. As samples, we take two typical resonator structures. For resonator 1, we assume that mirrors A and C are spherical with an identical radius of curvature r, and mirrors B and D are flat. For resonator 2, we assume that mirror A is spherical with radius of r and mirrors B, C and D are flat.

[a] e-mail: jlzhao@nwpu.edu.cn

2 Theoretical analysis

Under the paraxial approximation, the electric field of the laser beam in a nonplanar ring resonator can be described in cylindrical coordinates (r, ϕ, z) system by the expression [3,16]:

$$E = \frac{\sqrt{a^2 - b^2 - c^2}}{2} E_0 \exp\left[\mathrm{i}(kz - wt + \varphi)\right] \times \exp\left\{\frac{\mathrm{i}r^2\left[a + b\cos(2\phi) + c\sin(2\phi)\right]\pi}{2\lambda}\right\}, \quad (1)$$

where, $w = ck = 2\pi c/\lambda$ is the radian frequency, φ is the initial phase, a, b and c are the complex parameters of the laser beam, and z is the longitudinal coordinate.

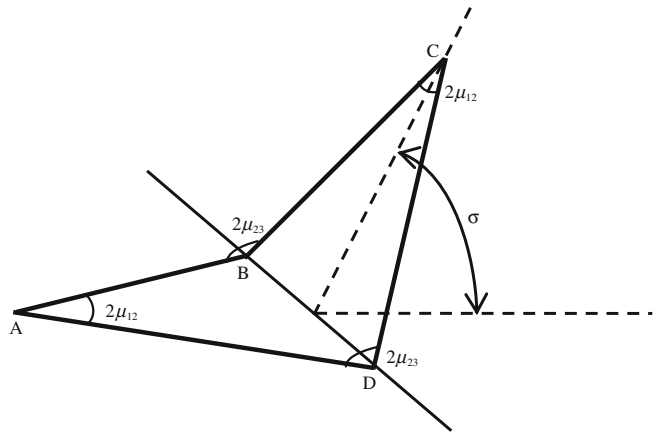

Fig. 1. Geometrical construction of a nonplanar ring resonator.

We use $R(\phi)$ and $\omega(\phi)$ to represent the wave-front radius of curvature and the beam size (measured at a position where the electric field amplitude drops to e^{-1} times of the maximum value E_0) in cross section, respectively. As we know, $\omega^{-2} > 0$ for physically reasonable beams. In general, the beam has elliptical contours of equal intensity (i.e., isophotes) and is astigmatic. The minor and major axes of the isophotes and the corresponding azimuthal coordinates can be calculated out by:

$$\frac{4}{k\omega^2} = \mathrm{Im}\, a \pm \sqrt{(\mathrm{Im}\, b)^2 + (\mathrm{Im}\, c)^2},$$
$$\Phi = \frac{\pi}{4} \pm \frac{\pi}{4} + \frac{1}{2}\arctan\frac{\mathrm{Im}\, c}{\mathrm{Im}\, b}. \quad (2)$$

Based on the analysis above, we know that the two principal wave-front radii of curvature are unequal, which can be presented as:

$$R^{-1} = \frac{\mathrm{Re}\, a \pm \sqrt{(\mathrm{Re}\, b)^2 + (\mathrm{Re}\, c)^2}}{2}. \quad (3)$$

Similarly, the azimuthal coordinates of the corresponding principal planes are given by:

$$\eta = \frac{\pi}{4} \pm \frac{\pi}{4} + \frac{1}{2}\arctan\frac{\mathrm{Re}\, c}{\mathrm{Re}\, b}. \quad (4)$$

Note that the corresponding signs in equations (3) and (4) must be identical if $\mathrm{Re}\, b > 0$, but opposite if $\mathrm{Re}\, b < 0$. In order to obtain the values of ω and R, we need to get the values of a, b and c, which can be calculated by using a set of transforms as:

$$d \equiv a^2 - b^2 - c^2, \quad (5)$$
$$\alpha \equiv a/d, \quad (6)$$
$$\beta \equiv b/d, \quad (7)$$
$$\gamma \equiv c/d, \quad (8)$$
$$\delta \equiv 1/d = \alpha^2 - \beta^2 - \gamma^2, \quad (9)$$

where, α, β, γ and δ depict the elements of vector $\mathbf{r}$, which is represented as $\mathbf{r} = [\alpha\ \beta\ \gamma\ \delta 1]^T$ and follows the matrix transformation:

$$\mathbf{r} = \mathbf{M}_i\mathbf{r}', \quad (10)$$

where, $\mathbf{r}'$ and $\mathbf{r}$ are the input and output beam vectors, respectively; $\mathbf{M}_i$ is the matrix for each ring resonator element including the surface reflection of a mirror, the translation along the optical axis and the beam rotation.

The reflection matrix of a spherical mirror with radius of r at the incident angle of μ is defined as:

$$\mathbf{M}(\mu, r) \equiv$$
$$\begin{bmatrix} 1 & 0 & 0 & -\frac{2}{r}\left(\frac{\cos^2\mu+1}{\cos\mu}\right) & 0 \\ 0 & 1 & 0 & -\frac{2}{r}\left(\frac{\cos^2\mu-1}{\cos\mu}\right) & 0 \\ 0 & 0 & -1 & 0 & 0 \\ 0 & 0 & 0 & 1 & 0 \\ -\frac{4}{r}\left(\frac{\cos^2\mu+1}{\cos\mu}\right) & \frac{4}{r}\left(\frac{\cos^2\mu-1}{\cos\mu}\right) & 0 & \frac{16}{r^2} & 1 \end{bmatrix}. \quad (11)$$

The matrix above can also be used to describe the reflection property of a plane mirror with the incident angle μ when $r \to \infty$. The matrices for the translation along the optical axis by l and the beam rotation about the optical axis by angle θ can also be defined tersely as $\mathbf{M}(l)$ and $\mathbf{M}(\theta)$ in reference [3].

The total round-trip matrix $\mathbf{M}$ for a resonator is the product of all individual element matrices $\mathbf{M}_i$ in proper sequential order:

$$\mathbf{M} = \prod \mathbf{M}_i. \quad (12)$$

Then we can obtain the equation based on self-consistent condition of the eigenmodes as following

$$\mathbf{M}\mathbf{r} = \lambda\mathbf{r}. \quad (13)$$

By solving equation (13), the eigenvectors of the matrix $\mathbf{M}$ can be obtained (including four beam solutions and one spurious solution). The values of a, b, c and d can also be obtained by substituting the eigenvectors into equations (5)–(8), then the size of eigenmodes in the elliptical cross section, the wave-front radius of curvature, as well as azimuths of the beam cross section and the phase contour can be obtained by substituting a, b and c into equations (2)–(4), respectively.

3 Propagation of the eigenmodes throughout the resonators

As we know that the eigenmode field in a nonplanar ring four-mirror resonator is an astigmatic Gaussian beam [17,18], which is characterized by following parameters: the sizes of the major and minor axes of the eigenmodes' cross section (ω_1 and ω_2), the wave-front radii of curvature (R_1^{-1} and R_2^{-1}), as well as azimuth angles between the major axis of the cross section of the eigenmodes and the corresponding contours of the equal phase (Φ and η). In the following, we analyze the beam parameters above versus the propagation distance throughout the resonators with two different structures in the case that the incident angles on the four mirrors are identical and the rotation angles of the resonators are 90° (the start

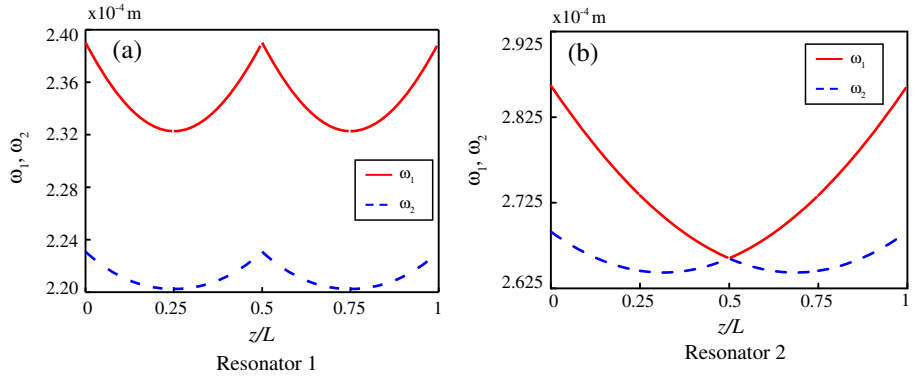

Fig. 2. Beam size of the cross section versus the propagation distance in resonators 1 (a) and 2 (b).

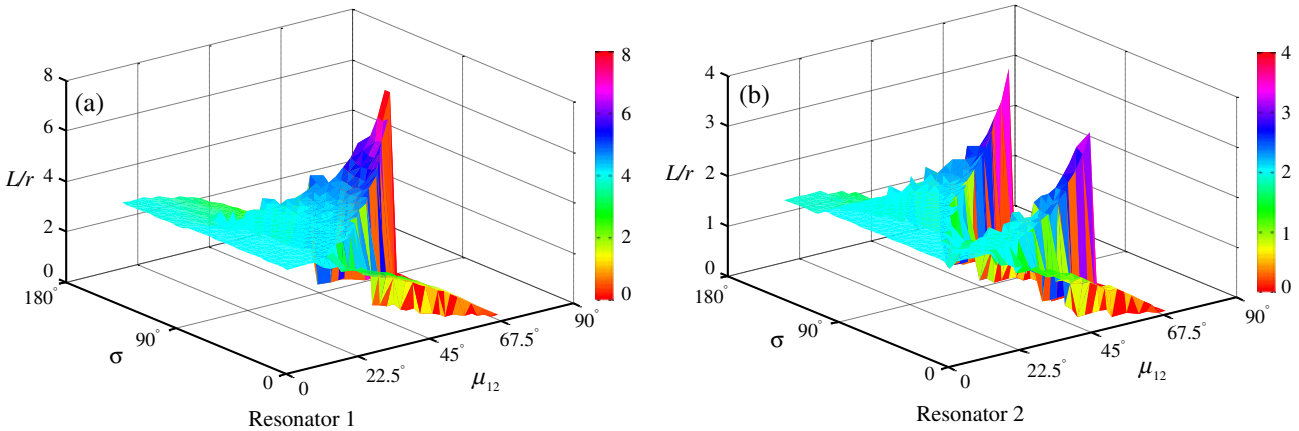

Fig. 3. Stability in three dimensions of resonators 1 (a) and 2 (b) versus L/r, incident angle μ and the folding angle σ.

point locates on the surface of mirror A, and the laser beam propagation direction is A → B → C → D → A).

Figure 2 presents the eigenmode sizes versus the propagation distance in resonators 1 and 2 (z means the distance from the surface of mirror A, and z/L is normalized). Where the adopted geometrical parameters are taken as following: $L/r = 0.1544$, $\lambda = 6.328 \times 10^{-7}$ m, $\sigma = 32.03°$ and $\mu = 43.87°$. It is shown that, in resonator 1 the sizes of the major and minor axes of the beam cross section change continuously throughout the resonator and reach the minimum ($\omega_1 = 2.32\times10^{-4}$ m, $\omega_2 = 2.20\times10^{-4}$ m) simultaneously on the surfaces of mirrors B and D, while they reach the maximum ($\omega_1 = 2.39 \times 10^{-4}$ m, $\omega_2 = 2.23 \times 10^{-4}$ m) on the surfaces of mirrors A and C (Fig. 2a). However, in resonator 2 the sizes of the major and minor axes can't reach the minimum at the same location. The size of the major axis reach the minimum ($\omega_1 = 2.66 \times 10^{-4}$ m) on the surface of mirror C, just the size of the minor axis ($\omega_1 = \omega_2 = 2.66 \times 10^{-4}$ m), which means the eigenmodes' cross section is an ideal circle at this location. The major and minor axes can reach their maximum ($\omega_1 = 2.86 \times 10^{-4}$ m, $\omega_2 = 2.69\times10^{-4}$) simultaneously on the surface of mirror A, and the beam sizes change continuously without any saltation on each mirror surface (Fig. 2b). It can be found that on each surface of the four mirrors in resonator 1, the sizes of the major and minor axes locate symmetrically at the same distance on both sides from it, but in resonator 2 this property can be valid only on the surfaces of the mirrors A and C.

Based on the analysis above, the influence of one or more structure parameters on the stability of a resonator can be judged qualitatively (the stable resonator with a satisfactory solution whose cross section $\omega^{-2} > 0$, or else the resonator is unstable). Figure 3 presents the stability of four-equal-sided nonplanar ring resonators 1 and 2 in three dimensions as a function of resonator structure parameters L/r, folding angle σ ($0 < \sigma < \pi$) and incident angle μ_{12} ($0 < \mu_{12} < \pi/2$). Under the chromatic surface, the resonators are stable, which means that the eigenmode's isophotes for both the major and the minor axes are finite. When either or both the axes of isophotes of the eigenmodes' are infinite in other regions, the resonators are unstable. The resulting stability surfaces, although complex, show that the resonator 1 can be stable with the largest structure parameter $L/r = 8$ for given incident angle and the folding angle ($\mu_{12} = 74.485°$, $\sigma = 91.671°$ or $\sigma = 85.944°$), but the resonator 2 can be stable only with a largest ratio $L/r = 4$ for an incident angle and the folding angle ($\mu_{12} = 74.485°$, $\sigma = 131.78°$). It can also be found that the volume of stability space of resonator 1 is larger than that of resonator 2 whether in the area $0 < L/r < 2$ (the traditional range, where the

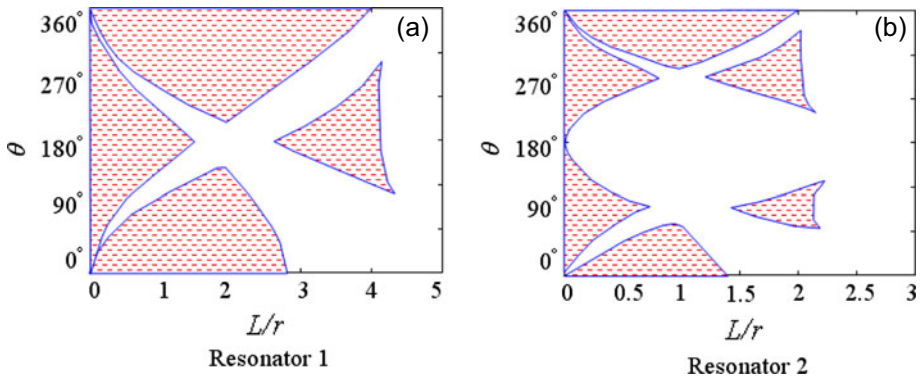

Fig. 4. Stability maps of resonators 1 (a) and 2 (b) (with the identical incident angles for all the four mirrors) versus L/r and θ.

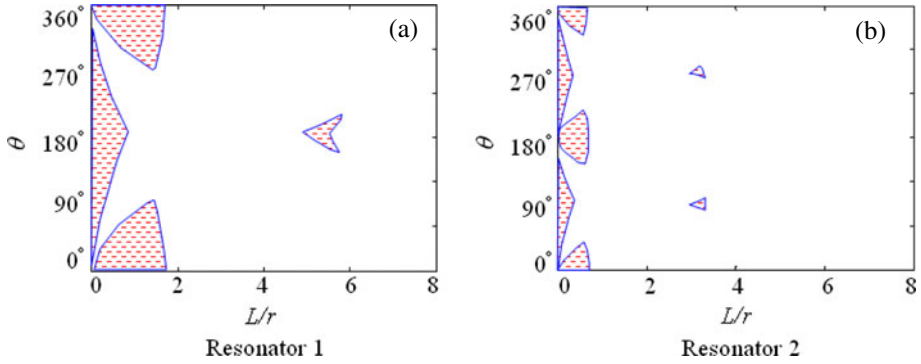

Fig. 5. Stability maps of resonators 1 (a) and 2 (b) (when the incident angles are unequal for the mirrors) versus the image rotation angle θ and L/r. The incident angles on mirror A are 65° and 70° in resonators 1 and 2, respectively.

resonator parameters of the ring laser gyroscope are located customarily [4]) or area $L/r > 2$ (the extended range, where the resonator parameters of the ring laser gyroscope are rarely located).

As we know, the relationships between the resonator parameters (folding angle, rotation angle and incident angles) can be expressed as:

$$\sin(\theta/4) = \tan(\mu_{12})\tan(\mu_{23}), \quad (14)$$
$$\cos(\sigma/2) = \sec(\mu_{12})\sin(\mu_{23}), \quad (15)$$
$$\sin(\mu_{12}) = \tan(\sigma/2)\tan(\theta/4), \quad (16)$$
$$\cos(\mu_{23}) = \sin(\sigma/2)\sec(\theta/4). \quad (17)$$

Combining with the stability condition and the relationship of the resonator parameters, we present the two-dimension stable area of these resonators versus L/r and the image rotation angle θ for more intuitively understanding the stability of these resonators. Figure 4 depicts the stability maps for resonators 1 and 2 with the identical incident angles (that means $0 < \mu = \mu_{12} = \mu_{23} < 45^\circ$ and the rotation angle range from 0 to 360° correspondingly) for all the four mirrors. It can be seen that the stable regions (shadow region) can be found only in the areas $0 < L/r < 4.5$ and $0 < L/r < 2.2$ for resonator 1 and 2, respectively. The stability map of resonator 1 is approximately symmetrical versus the image rotation angle from 0° to 360° and the area of the stability region of resonator 1 is larger than that of resonator 2. Unlike the case that the resonators with the identical angles, the stability region can also be found in the area $L/r > 4.5$ for resonator 1 and in the area $L/r > 2.2$ for resonator 2, when the incident angles of the four mirrors are unequal. Considering the influence from the rotation angle still further for a certain incident angle μ_{12}, Figure 5a shows the stability map for resonator 1 with certain incident angles (assumed $\mu_{12} = 65^\circ$ and the incident angle μ_{23} can be changed) on mirrors A and C versus the rotation angle from 0° to 360°. Similarly, Figure 5b shows the stability map for resonator 2 with certain incident angles (assumed $\mu_{12} = 70^\circ$ and the incident angle μ_{23} can be changed) on mirrors A and C versus the rotation angle from 0° to 360°. It can also be found that there are two stable regions in the area $2.2 < L/r < 4$ for resonator 2. Comparing with Figure 4, we can see that the incident angles on the mirrors in the resonators can also affect the stable area of the resonators evidently.

Figure 6 presents the wave-front radii of curvature R_1^{-1} and R_2^{-1} of the laser beam in resonators 1 and 2 (all the parameters adopted in this figure are same as Fig. 2). It can be seen that R_1^{-1} and R_2^{-1} in resonator 1 have a sudden change on the surfaces of mirrors A and C, but no change on the surfaces of mirrors B and D. One of the radii is negative and the other is positive when $0.175 < z/L < 0.325$ and $0.675 < z/L < 0.825$, while both R_1^{-1} and R_2^{-1} are negative when $0 < z/L < 0.175$ and $0.5 < z/L < 0.675$, but both positive in other locations

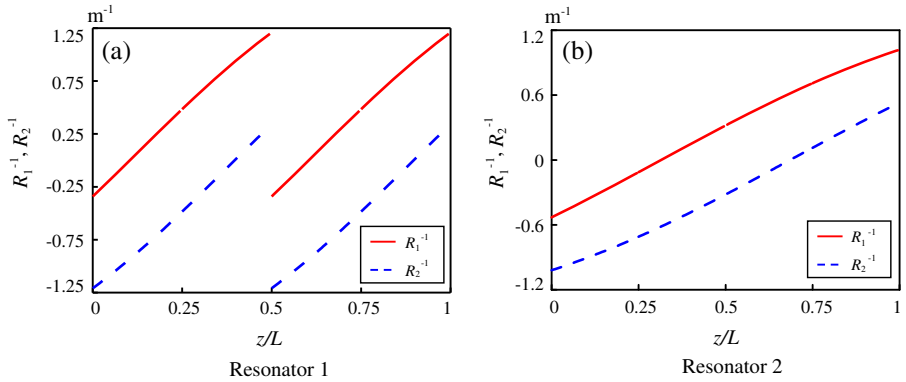

Fig. 6. Wave-front radii of curvature R_1^{-1} and R_2^{-1} of the laser beam versus the propagation distance in resonators 1 (a) and 2 (b).

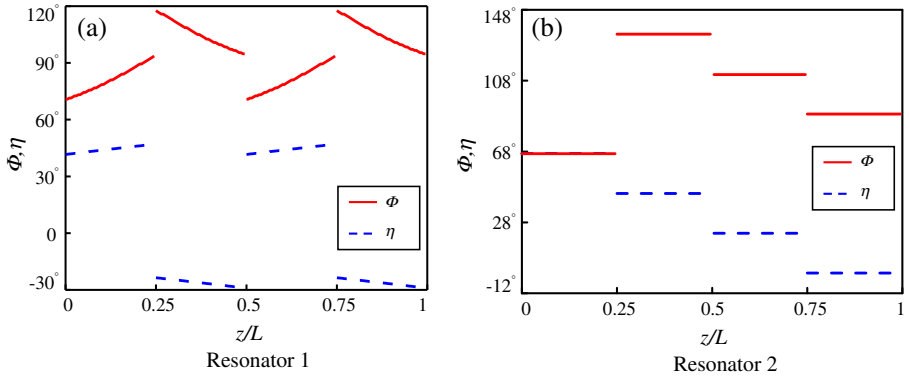

Fig. 7. Azimuths of the beam cross section and the phase contour versus the propagation distance in resonators 1 (a) and 2 (b).

throughout the resonator 1 (Fig. 6a). However, R_1^{-1} and R_2^{-1} change continuously throughout the resonator 2 except for the reflection on the surface of mirror A. It can be found that, one of the curvature is negative while the other is positive when $0.4 < z/L < 0.6$. Both R_1^{-1} and R_2^{-1} are negative when $0 < z/L < 0.4$ but positive in other locations throughout the resonator 2 (Fig. 6b). Based on the analysis above, we can confirm the shape of the wave-front intuitively, which is due to the fact that the wave-front is astigmatic protuberant Gauss surface with both positive radii but evidently astigmatic concave Gauss surface with the both negative radii of curvature R_1^{-1} and R_2^{-1}, and the wave-front is a hyperbolic paraboloid when R_1^{-1} and R_2^{-1} have opposite signs.

Figure 7 presents the azimuths of the beam cross section and the phase contour throughout the resonators (all the parameters adopted in this figure are same as Fig. 2). The azimuths of the beam cross section and the phase contour change continuously in free space between the two adjacent mirrors except for a saltation during the reflection on any surface of the four mirrors in resonator 1. The azimuth of the beam cross section varies more evidently than that of the phase contour (Fig. 7a). However, it is so special that the azimuths of the beam cross section and the phase contour remain unchanged in free space between the two adjacent mirrors in resonator 2 and they can also have a saltation during the reflection on the four mirrors (Fig. 7b), because the spherical mirror have the evident influence on the azimuths of the beam cross section and the phase contour. In the resonator, the spherical mirror A with radius of curvature r is equivalent to a focusing element with the focal axes F_x in principal plane xoz (meridional plane) and F_y in the other plane yoz (sagittal plane) for treating the astigmatism beam. The corresponding focal lengths in xoz and yoz planes are $f_x = 0.5\cos\mu_{12}$ and $f_y = r/(2\cos\mu_{12})$, respectively. The focusing impression on y-axis is more evident than that on x-axis (because $f_x < f_y$) during the reflection on the surface of mirror A, and the beam cross section of the eigenmode is elliptical. During the propagation between mirrors AB, focal axes F_x and F_y are identical with x- and y-axes of the beam cross section without any influence from other spherical mirrors in resonator 2. The rotation angles of focal axes F_x and F_y are identical to that of x- and y-axes of the beam cross section during the reflection on mirror B. Finally, the azimuth of the beam cross section is invariable during the space AB, BC and so on. Of course, the evolvements of the azimuth of the phase contour in a similar way in resonator 2. As we know, the diaphragm is elliptical in a nonplanar ring resonator, so it must be placed at the

location of the beam waist (its location close to a certain mirror shown as in Fig. 2). Notice that the azimuth of the diaphragm must match that of the beam both before and after the reflection on the mirror to filter the waves with certain frequencies. Therefore, these interesting results are important for designing and arranging the diaphragm of the ring resonators with nonplanar structure.

4 Conclusions

We have analyzed the propagation properties of the eigenmodes in general skew rhombus nonplanar ring resonators with two different structures systematically and presented stability in three dimensions of these four-equal-sided resonators as a function of L/r, the incident angle μ and the folding angle σ. The results show that for each mirror in resonator 1, the sizes of the major and minor axes locate symmetrically at the same distance on both sides from it, but in resonator 2 it can be valid only on the surfaces of the mirrors A and C. It is found the volume of stability space of resonator 1 is larger than that of resonator 2, and the resonator 1 can also be more stable than resonator 2 for a given incident angle. The results from the above comparison show that the influence originated from the nonplanar ring resonator geometry on the oscillation property of the laser beam evidently. We also analyzed the wave-front radius of curvature, as well as azimuths of the beam cross section and the phase contour in both of the two resonators. The calculation of the wave-front radius of curvature is useful for confirming the degree and the wave-front shape of the astigmatic Gauss beam. The azimuths of the beam cross section and the phase contour change continuously versus the propagation distance except for the reflection on the surfaces of the four mirrors in resonator 1. There are no image rotations in free space between two adjacent mirrors except for the reflection on the surfaces of the four mirrors in resonator 2. These interesting results are important for designing and arranging the diaphragm in the ring resonators with a nonplanar structure as well as optimizing the structure of the resonators themselves.

This work is supported by the Science Foundation of Aeronautics of China under Grant No. 20090853014 and the Northwestern Polytechnical University Foundation for Fundamental Research under Grant No. JC20110272.

References

1. W.W. Chow, J. Gea-Banacloche, L.M. Pedrotti, V.E. Sanders, W. Schleich, M.O. Scully, Rev. Mod. Phys. **57**, 61 (1985)
2. R. Rodloff, IEEE J. Quantum Electron. **23**, 438 (1987)
3. H. Statz, T.A. Dorschner, M. Holtz, I.W. Smith, in *Laser Handbook*, edited by M. Bass, M.L. Stitch (North Holland, 1985)
4. F. Zomer, Y. Fedala, N. Pavloff, V. Soskov, A. Variola, Appl. Opt. **48**, 6651 (2009)
5. Y. Honda, H. Shimizu, M. Fukuda, T. Omori, J. Urakawa, K. Sakaue, H. Sakai, N. Sasao, Opt. Commun. **282**, 3108 (2009)
6. G.B. Jacobs, Appl. Opt. **10**, 220 (1971)
7. D.D. Wen, D. Li, J.L. Zhao, Appl. Opt. **50**, 3057 (2011)
8. S.-C. Sheng, Opt. Lett. **19**, 683 (1994)
9. D.D. Wen, D. Li, J.L. Zhao, Opt. Express **19**, 19752 (2011)
10. J. Yuan, X.W. Long, M.X. Chen, Opt. Express **19**, 6762 (2011)
11. D. Li, D.D. Wen, J.L. Zhao, in *Proceeding of Internal Conference on Optical Instruments and Technology: Optoelectronic Measurement Technology and Systems, Beijing 2011*, edited by X. Dong, X. Bao, P.P. Shum, T. Liu (SPIE, 2011), p. 82010M-1
12. J.A. Arnaud, Appl. Opt. **9**, 1192 (1970)
13. A.H. Paxton, W.P. Latham Jr., Appl. Opt. **25**, 2939 (1986)
14. A.E. Siegman, IEEE J. Sel. Top. Quantum Electron. **6**, 1389 (2000)
15. A.B. Plachenov, V.N. Kudashov, A.M. Radin, Quantum Electron. **39**, 261 (2009)
16. J. Yuan, X.W. Long, L.M. Liang, B. Zhang, F. Wang, H.C. Zhao, Appl. Opt. **46**, 2980 (2007)
17. Y.Y. Broslavets, T.E. Zaitseva, A.A. Kazakov, A.A. Fomichev, Quantum Electron. **36**, 447 (2006)
18. I.V. Golovnin, A.I. Kovrigin, A.N. Konovalov, G.D. Laptev, Quantum Electron. **25**, 436 (1995)

Appendix

Tables 1 and 2 present the values of beam parameters (the cross section size and the wave-front radius of curvature of the eigenmodes) on the surfaces of all the four mirrors within both the two different resonators to present a better apprehensible of the eigenmodes' polarization properties for the reader. All the parameters to define the geometrical structure are taken as following: the total resonator length $L = 0.21$ m, the curvature radius of the mirror $r = 1.36$ m, the folding angle $\sigma = 32.03°$ and incident angles $\mu = 43.87°$.

Table 1. Beam parameters on the surfaces of all the four mirrors in Resonator 1.

Mirror i / Beam parameters	A	B	C	D
ω_1 ($\times 10^{-4}$ m)	2.23088	2.20242	2.23088	2.20242
ω_2 ($\times 10^{-4}$ m)	2.39026	2.32273	2.39026	2.32273
R_1^{-1}	−0.34138	0.48410	−0.34138	0.48410
R_2^{-1}	−1.20865	−0.48410	−1.20865	−0.48410

Table 2. Beam parameters on the surfaces of all the four mirrors in Resonator 2.

Mirror i / Beam parameters	A	B	C	D
ω_1 ($\times 10^{-4}$ m)	2.69110	2.64555	2.65919	2.64555
ω_2 ($\times 10^{-4}$ m)	2.86183	2.73368	2.66097	2.73368
${R_1}^{-1}$	−0.53008	−0.11299	0.3274	0.70994
${R_2}^{-1}$	−1.01995	−0.70994	−0.3106	0.11299